A Tripodal Molecule on a Gold Surface: Orientation-Dependent Coupling and Electronic Properties of the Molecular Legs

Maya Lukas,[†,⊥,*] Kerrin Dössel,[†,⊥] Alexandrina Schramm,[†] Olaf Fuhr,[†,⊥] Christophe Stroh,[†] Marcel Mayor,[†,‡,⊥] Karin Fink,[†] and Hilbert v. Löhneysen[†,§,⊥]

[†]Institute of Nanotechnology, Karlsruhe Institute of Technology (KIT), D-76021 Karlsruhe, Germany, [‡]Department of Chemistry, University of Basel, CH-4056 Basel, Switzerland, [§]Physics Institute and Institute for Solid State Physics, Karlsruhe Institute of Technology (KIT), D-76049 Karlsruhe, Germany, and [⊥]DFG Center for Functional Nanostructures (CFN), D-76049 Karlsruhe, Germany

ABSTRACT The realization of molecular electronics demands a detailed knowledge of the correlation between chemical groups and electronic function. It has become obvious during the last years that the conformation of a molecule and its coupling to the connecting electrodes plays a crucial role in its conductance behavior and its electronic function, *e.g.*, as a switch. Knowledge about these relationships is therefore essential for future design of molecular electronic building blocks. We present a new three-dimensional molecule, consisting of three identical molecular wires connected to a headgroup. Due to the well-defined spatial arrangement of the molecule in a nonplanar geometry, it is possible to investigate the conductance behavior of these wires with respect to their position and coupling to the surface electrode with the submolecular resolution of a scanning tunneling microscope. The experimental findings are supported by calculations of the electronic structure and conformation of the molecule on the surface by density functional theory with dispersion corrections.

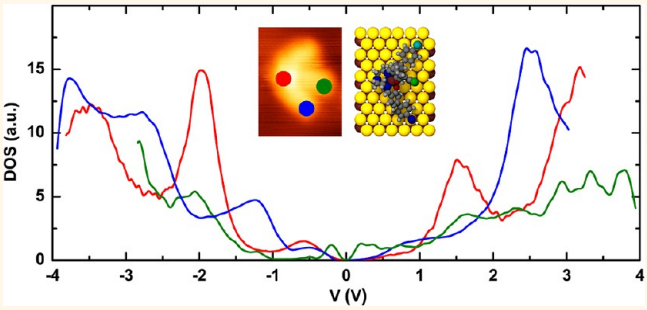

KEYWORDS: molecular electronics · multiterminal molecule · single-molecule junction · submolecular resolution · scanning tunneling spectroscopy · density functional theory

In recent years the field of molecular electronics experienced a boost. Although molecular applications in electronics require self-assembled multimolecular structures rather than single molecular junctions, the knowledge about the fundamental correlations between a molecule's functional chemical groups, its contacts, and surroundings and the resulting electronic properties is imperative for the designing of future molecular electronic building blocks.[1−16] These fundamental correlations have been studied in recent years mainly by inserting molecules into mechanically controlled (MCBJ) and other break junctions techniques[1,2,4−7,11,16−18] or by scanning tunneling microscopy (STM).[12−15] While in MCBJ high stability of the contacts is achieved and all break junction experiments deliver very good measurement statistics, little is known about the configuration of the molecule and the contacts.[11,16−19] These decisive aspects can in principle be investigated by STM and scanning tunneling spectroscopy (STS).[11−15,20−22] However, wire-like molecules tend to adsorb with their long axis parallel to metallic surfaces, making transport measurement along the wire axis impossible. Picking the molecular wire up from the surface by an STM tip[5,11,12,15] changes not only its bonding to the electrode but very likely also the conformation of the molecule itself. This manipulation therefore frustrates the original potential of the STM method to characterize both molecule and contact. It is, however, highly desirable to characterize the molecular contact in the very same configuration as that of the electronic measurement. A multipodal molecular "stand" may therefore be used to lift molecular wires or functional units permanently from the surface.[18,23−30] Most studies on such molecules used ensemble averaging methods, *e.g.*, XPS, cyclic voltamogrammetry, and luminescence. Local

* Address correspondence to maya.lukas@kit.edu.

Received for review April 24, 2013 and accepted June 22, 2013.

Published online June 22, 2013
10.1021/nn4020505

orientational and conformational properties on single molecules were scarcely investigated,[23,27] and the only investigation of electronic transport through a single tripodal molecule used a break junction technique.[18]

To enable unprecedented insight into the relation between the molecular wire's conformation and orientation to the surface and its electronic transport properties, we designed molecules that adopt a tripodal form, preventing a configuration where the molecule lies flat on the metal surface,[31,32] and investigated them by STM and STS with submolecular resolution. Here, we report on an investigation of a gallium complex comprising such a rigid three-dimensional structure. After deposition on a Au(111) surface, some of the wire-like parts of the molecule will protrude freely, becoming accessible for investigation with an STM tip. We demonstrate by STS measurements in combination with density functional theory (DFT) calculations that substructures that are chemically identical in solution become distinguishable upon adsorption; that is, they exhibit strongly varying electronic properties that depend on their different orientation with respect to the surface and arise from different coupling to the metal surface. It is, to our knowledge, the first time that the electronic properties of an elongated conjugated molecular wire are shown for isolated single molecules with respect to their *a priori* well-determined conformation and orientation toward the surface.

RESULTS AND DISCUSSION

To form a tripodal molecule, three identical molecular wires ("legs") are rigidly attached to a Ga^{III} complex ("head"), as shown in Figure 1(a), with the resulting structure determined by single-crystal X-ray diffraction in Figure 1(b).[31] All rotations possible within the molecule preserve its three-dimensional structure. Consequently, the molecule must protrude from a planar surface, either with its head when standing on all three legs or with one leg when lying "on the side". Figure 1(c) shows a typical STM image of a Au(111) surface covered by a submonolayer of these molecules deposited from solution at room temperature (see Methods section for details).

In spite of a rather weak molecule−substrate interaction that preserves the Au herringbone reconstruction,[33] the molecule positions are stable at the measuring temperature of 30 K. They preferably bind near the "elbows" and in the fcc regions of the Au surface, whereas the hcp regions are less frequently occupied, as can be seen in the inverted-height-scale image in Figure 1(d). At low coverages the transition regions between the fcc and hcp regions of the herringbone reconstruction are not covered at all.

The fraction of molecules binding with all three legs to the surface (Figure 1(e)), *i.e.* in the configuration of a molecular "lunar module" as shown in the schematic of Figure 1(f), is very small (≤1%). The bonding configuration shown in Figure 1(g) represents the most frequently observed type. The size and angular structure of this image suggest that this is a tilted "lunar module": Starting from a "lunar module", two sulfur positions are fixed and the molecule is rotated around the axis connecting the fixed sulfur atoms. This lifts the third leg from the surface, while it brings the two legs with the sulfur atoms attached to the surface and the headgroup closer to the surface. Such a tilted molecule is shown in the schematic picture of Figure 1(h). The projection to the surface resembles an angulate sign ∈, where the middle bar is the leg that is pointing away from the surface (middle leg), while the angulate outer frame ⊂ is given by the head and the legs that are tilted toward the surface (side legs).

In some cases we observe features in the STM images that cannot be identified as intact molecules, *e.g.*, the lower of the two features in the upper right-hand corner of Figure 1(d). In order to check if these features arise from disintegration of molecules during deposition, we performed STM investigations after the deposition of the leg group only. In this case we observe structures completely different from the ones identified as intact molecules but also different from the features just mentioned.[31] Furthermore, after deposition of molecules we find no areas similar to the Ga islands or alloyed Au areas reported in ref 34. Therefore we suppose that the structures frequently found still contain the metal ion in its head complex and that Figure 1(g) indeed shows an intact tripod.

To gain insight into the electronic structure of the molecule in this nonsymmetric orientation with respect to the surface, we performed current−voltage, $I(V)$, measurements at well-defined positions above the molecule, always maintaining a vacuum gap between tip and sample. It must be noted that the molecule has C_3 symmetry and is chiral, with a racemic mixture of both enantiomers. In the tilted orientation (Figure 1(g)), each of the three chemically identical legs adopts a different orientation with respect to the surface. We are, however, not able to distinguish between the two side legs on the basis of the STM images alone. Therefore, $I(V)$ curves were measured either above the head, the protruding middle leg, or the side legs, without distinguishing between the side legs at this point.

For the rather large voltage ranges used in the spectroscopy of molecules, dI/dV cannot be interpreted as a quantity proportional to the sample's local density of states (DOS).[35−38] We therefore deconvolved the DOS by the method proposed in ref 35 (for details see the Methods section). The resulting spectra are shown in Figure 2 for the different positions indicated by colored dots in the inset. Peaks in the deconvolved DOS do reflect the energy positions of electronic states correctly; however, the relative height

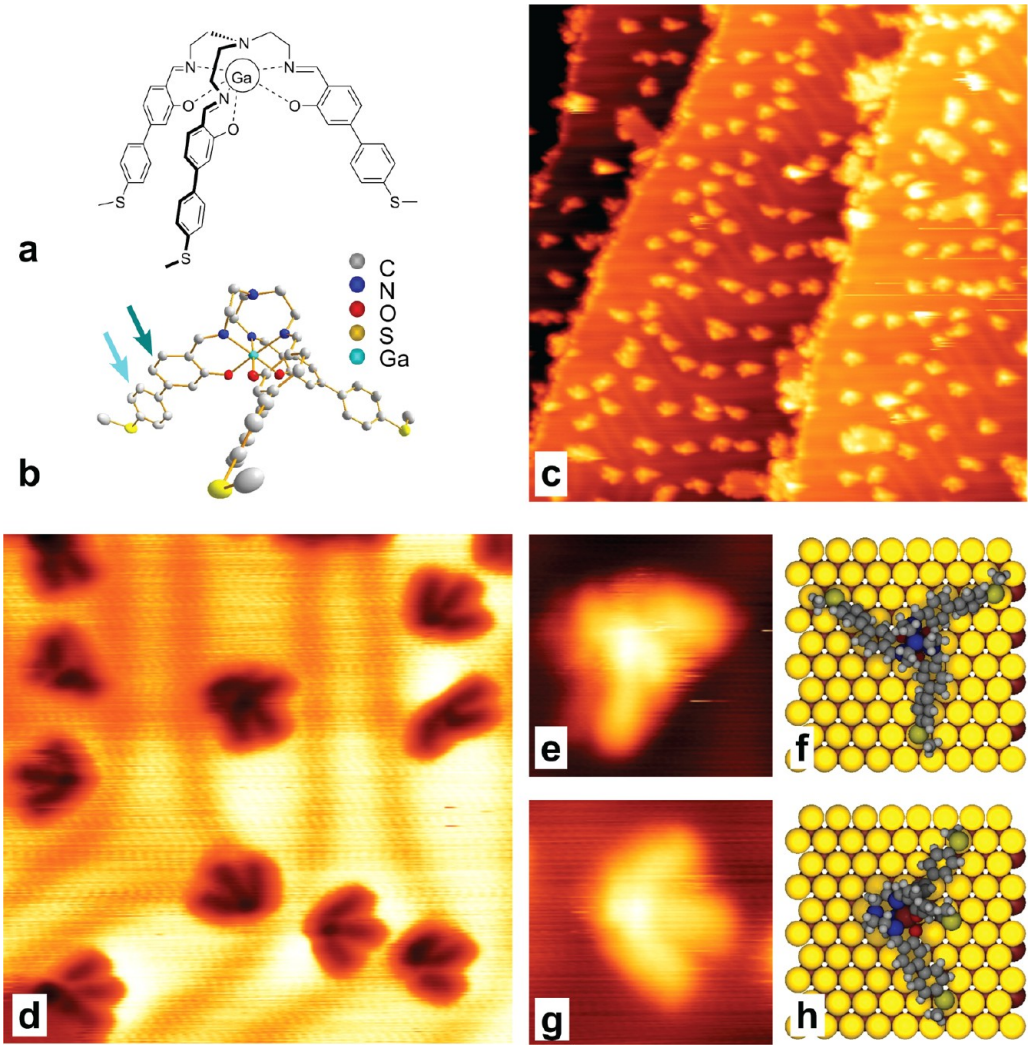

Figure 1. Structure and STM imaging of the tripodal molecule. (a) Chemical molecular structure and (b) structure of the molecule as found by X-ray diffraction.[31] The arrows mark the "upper" (dark cyan) and "lower" (light cyan) phenyl ring of the leg. (c) Submonolayer of tripodal molecules on Au(111). (d) Inverted-height-scale image. The transition lines between fcc and hcp regions of the herringbone reconstruction appear as dark lines. Molecules mainly bind at the elbows and in the fcc regions. (e) Molecule in a standing "lunar module" configuration (the symmetry in this high-resolution image suffers due to piezo-creep) and in a (g) tilted configuration. (f) Schematic of the "lunar module" configuration and (h) tilted configuration. STM images in constant current mode: V = 2 V, I = 23 pA. Image widths: (c) 90 nm; (d) 21 nm; (e and g) 5 nm.

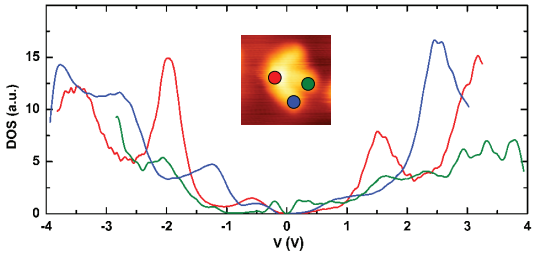

Figure 2. DOS spectra obtained from the local $I(V)$ measurements on the head (red), side (blue), and middle leg (green).

of two peaks does not yield unambigous information on the relative weight of the corresponding states in the real DOS.[35]

It can clearly be seen that the prominent features in the measured DOS differ for different positions of the STM tip above the molecule. Spectra on the head and the side leg seem to have nearly opposite behavior: when a maximum is observed on the head, a minimum is found near that energy on the side leg (*cf.* ∼−2 V, 1.7 V, 3 V) and *vice versa* (*cf.* ∼−2.7 V, −1.2 V, +2.3 V). On the other hand, the spectra on the middle leg show peaks at similar energies to the head.

A few conclusions can be drawn from the measured spectra right away: Without coupling to a surface all three legs are identical and similar spectra should be obtained on the middle and the side legs. In the tilted configuration of Figure 1(h) all three legs couple differently to the surface. The strong differences in the spectra on the middle and side leg immediately show the effect of the surface on the electronic structure of the leg. As mentioned above, possible differences in

the spectra between the two side legs are not resolved with our tip (which remains at RT while the sample is cooled). Second, the fact that spectra on the middle leg resemble the spectra on the head suggests that there exist orbitals that extend over the head and middle leg. Hence electrons are able to tunnel resonantly through the leg and head, *i.e.*, "along" the middle leg, at the corresponding energies. Third, since the spectra on the side legs exhibit minima at the main peaks of the head (−2 V, 1.7 V, 3 V) and, conversely, maxima at energies of minima on the head (−2.7 V, −1.2 V, +2.3 V), orbitals located at both the head and side leg at the same energy seem to be scarce. Therefore elastic transport along the side leg to the head is not possible, and electrons emitted from the tip have to tunnel "across" the side leg directly into the surface.

We conclude that the different coupling of the wires to the surface enables two different electron pathways through the molecule: "along" the leg for the middle leg and "transversing" the leg for the side leg. (We note that the concept of "tunneling along" or "across" strictly speaking does not hold for an electron occupying an orbital with spatially dependent probability amplitude. With the term "tunneling along" we refer to the process where the electron enters the molecular orbital at the leg and exits the molecule at the head.)

To test our interpretation of different electron pathways through the molecule, we performed quantum chemical calculations (for details see the Methods section) and analyzed the electronic structure of the molecule with different conformations and surroundings: (a) the isolated and relaxed molecule (gas phase molecule), (b) the molecule fixed in the distorted conformation that it adopts upon adsorption at the gold surface, but without the surface (distorted gas phase), (c) the molecule in distorted conformation with the gold surface at 26.5 nm distance, and (d) the molecule adsorbed at the gold surface (distorted/relaxed molecule on the surface). The surface was modeled by two layers of 10 × 10 Au atoms. The Au positions were kept fixed at the positions of an unreconstructed Au(111) surface. For (a) and (d) the structure of the adsorbed molecule was optimized. The distorted conformation after relaxation on the surface (d) was kept fixed to calculate (b) and (c). Since the system is rather large, typically leading to a large number of local minima, information from the STM measurements is needed to come up with a reasonable starting configuration.

To this end, we investigated the molecule's orientation with respect to the herringbone reconstruction. The orientation of the gold reconstruction was inferred from the transition lines and its behavior at the step edges.[39] We define the orientation angle α as the angle between the bisectrix of the side legs and the transition line as shown in Figure 3(a). The angles β and γ (see Figure 3(a)) depend strongly on the exact definition of the head position (*i.e.*, intersection point of the lines through the side legs). However the bisectrix (and hence α) is much less affected by this uncertainty.

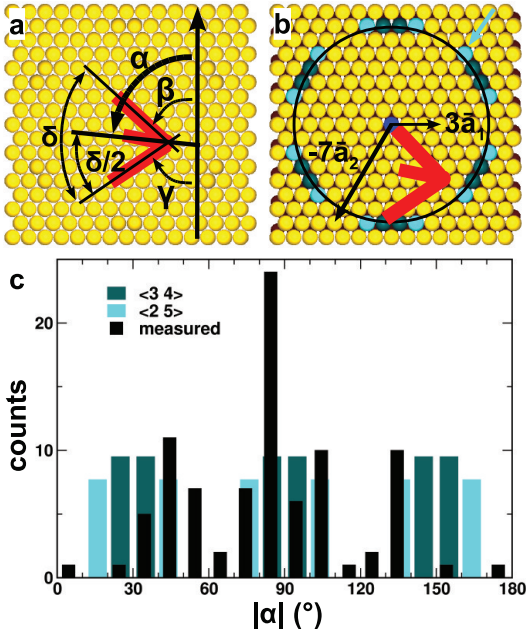

Figure 3. Orientation of molecules. (a) The orientation of a molecule is determined by the angle α between the bisectrix of the side legs and the direction of the herringbone transition lines (long vertical arrow). The observed values are given by black bars in (c). (b) Orientations are named by the vector connecting the sulfur atoms of leg 1 (blue) and leg 2 (cyan). For example, the orientation of the schematically drawn molecule is [3 −7]. The circle indicates the S−S distance found in the X-ray crystal structure of the molecule. Atoms marked in dark and light cyan are the most probable positions for the second sulfur atom; the light cyan arrow indicates the orientation [2 5]. The theoretical probabilities for these orientations are indicated in (c) as colored bars.

The distribution of angles α as found on our samples is given by the black bars in Figure 3(c). Molecules at elbow sites were not included. We also indicate a "probability" for two different orientations called <2 5> and <3 4>, which are determined as follows: From the X-ray structure of molecular crystals the distance between the sulfur atoms of the legs is given by 1.72 nm.

If we position one sulfur at a certain position on the gold surface (blue "atom" in the center of Figure 3(b)), then the ideal distance for the sulfur atom of the second leg is given by the black circle line. Only a few positions exist where the sulfur atom of leg 2 can be accommodated in a position with identical site symmetry to that of leg 1 without much expansive or compressive strain on the molecule. The orientations with least strain are the families of <6 0>, <3 4>, and <2 5> orientations, where <*a b*> indicates all orientations where the sulfur of leg 2 is found at a position $\pm(a\mathbf{a}_i\ b\mathbf{a}_j)$ from the sulfur of leg 1, with $\mathbf{a}_{i,j}$ being any two of the hexagonal unit vectors of the (unreconstructed) surface. The respective positions are indicated

in Figure 3(b) as light and dark cyan "atoms" for <2 5> and <3 4> orientations, respectively. The exact orientation [a b] refers to the specific choice of hexagonal unit vectors given in Figure 3(b).

Stretching or compressing the molecule by a distance δ will result in an energy penalty that exponentially reduces the probabilty to find this conformation (for details see the Methods section). These theoretical probabilities are shown as colored bars in Figure 3(c). For clarity the orientation that—based on this stretching energy argument—should be the most probable (<6 0> at multiples of 60°) is not shown because it is not adopted by the molecules at all.

It is evident that orientations with the same probability based on the S−S distance (bars of same color in Figure 3(c)) are not observed with the same probability in the experiment. We attribute these differences to the interaction of the whole molecule with the surface, which has not been considered so far. Taking the interaction with the gold surface into account, a few things have to be considered: First, orientations rotated by 60° are not identical if the second gold layer matters, while orientations rotated by 120° are identical when the Au surface reconstruction is neglegted. Furthermore, an orientation of a right-handed (R) molecule on the surface at angle α is the mirror image of a left-handed (L) molecule on the surface at angle $-\alpha$. Mirror imaging the complete system does not change its energy; hence the identical configurations (R, α) and (L, $-\alpha$) have the same energy and hence the same probability. On the other hand, (R, α) and (R, $-\alpha$) are not identical configurations and may therefore have different energy and probability. The molecules in our samples exist in a racemic mixture, and all of the four configurations (R/L, $+\alpha/-\alpha$) may exist. However, we are not able to distinguish R and L species in the STM images; therefore we cannot distinguish (R, $-\alpha$) from (L, $-\alpha$), and hence it is not useful to discriminate probabilities for α from those for $-\alpha$. Accordingly, we show the orientations over $|\alpha|$ in Figure 3(c).

It is conspicious that not all of the three orientations rotated by 120° are found in the experiment. We attribute this to the herringbone reconstruction, which breaks the 3-fold symmetry. For example, the angles $+85°$, $-35°$, and $-155°$ are identical orientations on an unreconstructed surface. However, for $-155°$ or $-35°$ the head of the molecule would be positioned far away from the transition lines in order to place the complete molecule inside the fcc region of the reconstructed surface, an orientation that is virtually never observed. The head is always oriented toward a transition line or toward the kink of an elbow, which therefore seems to be energetically favorable. If the head was placed in the vicinity of the transition region at this angle, one of the legs would extend into the transition region, which apparently is unfavorable as well. We therefore attribute the missing of orientations

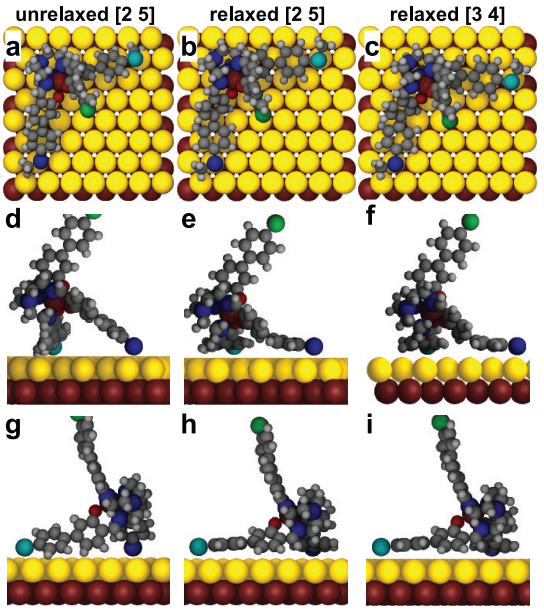

Figure 4. Positions of molecules: (a−c) top and (d−i) side views of the molecule. The left column shows the unrelaxed molecule. The center and right column show two structures after relaxation. The sulfur atoms of leg 1 (blue), leg 2 (cyan), and the protruding leg (green) are marked with color to clarify the orientations in the side views. The CH_3 groups attached to the sulfur atoms are not shown in the side views for clarity.

with small angles below 40° and of angles in the range 140−180° to the interaction with the transition region.

Having identified the most probable orientations from experiment, we chose the starting orientation for the DFT calculations: We positioned two sulfur atoms of the molecule nearly on top of gold atoms in a <3 4> or <2 5> orientation and tilted the molecule around the S−S axis so that the view from above resembles the shape we see in the STM. The [2 5] starting orientation is shown in Figure 4(a) seen from above and (d,g) from two sides. Figure 4(b,e,h) show the molecule after relaxation from the initial structure. Finally, Figure 4(c,f,i) show a structure relaxed from the [3 4] starting position. The sulfur atoms are shown in cyan, blue, and green for legs 1−3 to enable better identification of the orientation in the side views. For clarity the methyl groups attached to the sulfur are not shown in the side views. In the following the phenyl rings of one leg are referred to as "lower" and "upper" (see Figure 1(b)). Our calculations show the following main features: The "lower" phenyl ring of leg 2 (cyan) is tilted in all final configurations, probably to bring its π system into stronger overlap with the surface electron system. Leg 1 (blue) cannot bring the lower phenyl ring parallel to the surface by rotation of the ring alone. Instead, the adjustment is reached by a distortion of the whole leg. This brings the Ga complex closer to the surface and aligns the π system of leg 1 more parallel to the surface. The sulfur atoms prefer a nearly on-top

TABLE 1. Distances and Energies for the Relaxed Structures

			distance (pm)		
group	configuration	angle (deg)	S_1—Au	S_2—Au	relative energy ΔE (eV)
<3 4>	**[3 −7]**, [−7 4], [4 3]	+**85**, −35, −155	257	270	2.54
<3 4>	**[4 −7]**, [−7 3], [3 4]	+**95**, −25, −145	266	279	0.86
<2 5>	**[2 −7]**, [−7 5], [5 2]	+76, −**44**, −164	268	280	0.00
<2 5>	**[5 −7]**, [−7 2], [2 5]	+**104**, −16, −136	263	269	0.73

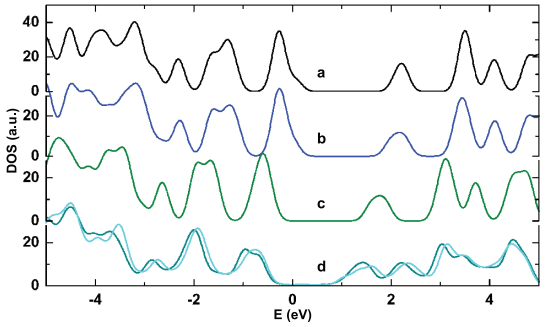

Figure 5. Calculated DOS for the complete molecule for (a) the isolated molecule, (b) the distorted [5 2] conformation without surface, (c) the distorted [5 2] conformation with surface at 26.5 nm distance, and (d) distorted [5 2] (cyan) and [3 4] (dark cyan) conformation with surface, *i.e.*, the molecule relaxed on the surface.

position. The S—Au distances, given in Table 1, are in the range of typical S—Au binding distances. The relative energies of the different configurations with respect to the lowest energy structure found are given in Table 1 as well.

In order to understand the effect of the surface on the electronic properties of the molecule, we extract the total density of states of the molecule from the DOS of the system including the surface by summing the population stemming from molecular atoms. The resulting discrete orbital energy spectrum is broadened by ΔV = 0.3 eV, which is in the range of the experimentally observed peak widths (for details see the Methods section).

To distinguish the effect of the geometric distortion from that of the vicinity of a metallic electrode, we calculated the electronic structures of (a) the isolated molecule, (b) the isolated molecule in the distorted conformation [5 2], (c) the distorted conformation [5 2] with the surface at 26.5 nm distance, and (d) the distorted conformations [5 2] and [3 4] of the molecule adsorbed at the surface. The extracted molecular DOS is shown in Figure 5(a—d), respectively. The alteration of the DOS due to the distortion of the molecule is small. The relative weight of the peaks does change somewhat, but the peak positions are affected only a little (Figure 5(b)). When the surface is included in the calculations, the Fermi levels of the molecule and the metal cluster have to adjust. At long distances (26.5 nm) this is realized in the calculations by a very small electron transfer from the molecule to the metal cluster (0.17 electron). Therefore, the positions of all peaks originating from the molecule shift to lower energy (Figure 5(c)) even with the surface being at large distance. The fact that the double peak structure at −1.6 eV/−1.3 eV not only shifts but also narrows somewhat indicates that the energetic shift can be different for different orbitals. Finally, adsorbing the molecule at the surface results in a further energy shift but also in the occurrence of new features, *e.g.*, an additional peak at positive energy (unoccupied orbitals) between the two first peaks in Figure 5(d). The difference between the configurations [3 4] and [5 2] marked as dark and light cyan is small.

In order to elucidate the effect of the gold surface on different orbitals of the molecule, we performed the summation over orbitals for parts of the molecule only to obtain a local (L) DOS, which can be compared with the experimental curves. We assign groups of atoms to belong either to one of the legs or to the head and sum over the orbitals belonging to atoms of the respective group only. We calculated the LDOS for different distributions of atoms to the head and the three leg groups. Two of these distributions are shown in Figure 6.

In distribution I only the lower phenyl ring and the thiomethane group are included in the leg groups, while all other atoms are added to the head. The respective spectra are drawn in light colors in Figure 6; the atoms that contribute to the respective spectrum are colored in the inset. Distribution II includes both phenyl rings and the oxygen atom in the leg groups, while all remaining atoms contribute to the head. The LDOS for this distribution is shown in dark colors in Figure 6.

The effect of the grouping of atoms either to the leg or to the head is very prominently seen, for example, for the peak at −1 eV. "Removing" the contribution of the upper phenyl ring, *i.e.*, going from II to I for a leg, leads to a strong reduction of the peak. Hence the orbitals of the upper phenyl ring are the main contributers to this peak. This effect is most pronounced for the side legs. For the middle leg this peak is found in the spectrum of distribution I as well, while it is strongly surpressed for side leg 1 and completely vanishes for side leg 2, which has its lower phenyl ring most parallel to the surface. Apparently, the stronger the interaction with

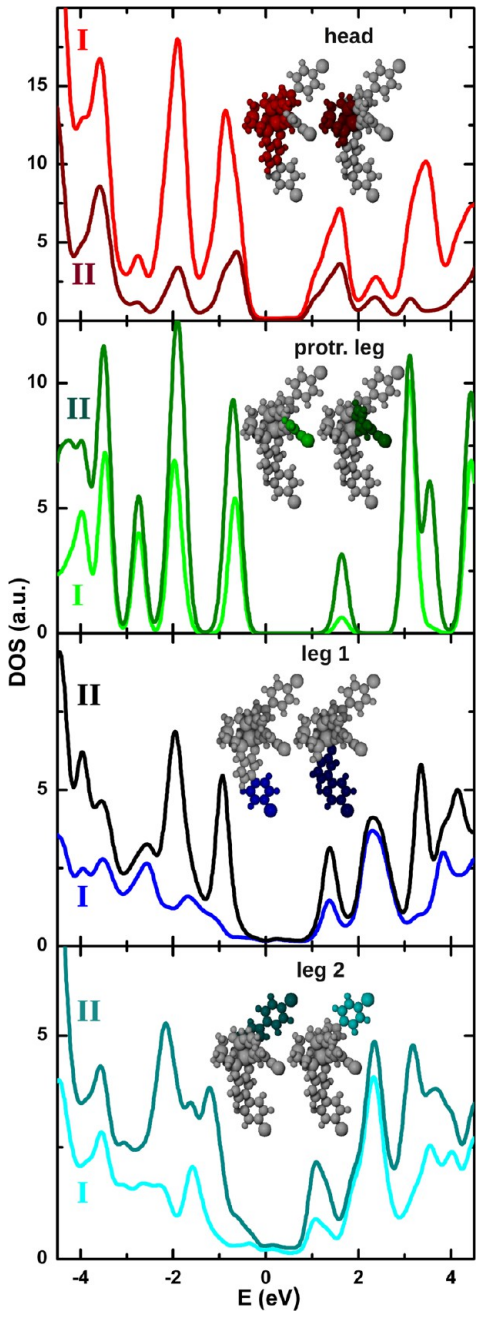

Figure 6. Calculated local DOS of conformation [5 2] for distributions I (light colors) and II (dark colors). The atoms contributing to the respective LDOS in distributions I and II are marked with light and dark colors, respectively, in the inset.

the surface, the less the contribution of the upper phenyl ring at −1 eV.

Another example for the strong effect of the surface is the peak at +3 eV (middle leg)/+2.5 eV (side legs). It obviously arises mainly from orbitals of the lower phenyl ring. Therefore, the LDOS hardly changes between I and II. However, the energy position of this peak depends on the coupling to the surface. For the two side legs the peak energy is shifted with respect to that of the middle leg. This shift is strongest for leg 2, which has its phenyl ring more parallel to the surface. It also emerges that the "new" peak occurring in Figure 5(d) is due to those orbitals at the side legs that shift in energy due to their interaction with the surface.

All pronounced head orbitals seem to extend to the upper phenyl rings as well. But the two aforementioned effects, a strong shift of peaks stemming from unoccupied orbitals at the lower phenyl rings and, second, the marginal contribution of the lower phenyl rings to some peaks, are found for the side legs but not for the middle leg. Therefore, the spectra of the head and middle leg resemble each other much more closely than those of the head and side legs in distribution I.

In Figure 7 we finally compare the calculated local spectra with the measured local DOS. We show the head and middle leg spectra on the left and the side leg spectra on the right. The middle panel contains measured spectra. The upper and lower panel show the calculated DOS for distributions I and II, respectively. Overall there is a good agreement between the measured spectra and the calculated DOS. We point out that there is no arbitrary adjustment of the Fermi energy (E_F) in the theoretical spectra. The highest occupied molecular orbital (HOMO) of the isolated molecule has been set as E_F. The resulting work function $\phi = 4.635$ eV is then used as a shift for all calculated spectra (see Methods section). The agreement of the calculated and measured energies without further adjustment is remarkably good. However, much more important, the trend in how peak positions shift for different positions of the tip above the molecule is in agreement with the shifts found in the calculations, as will be discussed in the following.

For spectra on the head all measured peaks are resembled in the calculation of the DOS. The spectrum of occupied head states was measured at the position indicated with a cross in the inset, *i.e.*, on the bright dot, away from the leg structures. Spectra taken closer to the border between the bright dot and the leg better fit to those of the side legs. We therefore conclude that the bright dot seen in the STM images arises from the molecular complex coordinating the Ga atom, but does not contain the upper phenyl ring.

For spectra collected on the middle leg we find good agreement with the calculated spectra; however the measurements at small energies were hampered by a very large distance between tip and sample ($V \approx 2-2.5$ eV and $I \approx 20-30$ pA before freezing the feedback loop). For smaller distances we would manipulate the molecule during an $I(V)$ measurement. Due to the weak interaction of the middle leg with the surface, the molecule will couple to the tip and be lifted from its position or even transferred to the tip at larger voltages when the tip is too close. At the required large distances, we are at the resolution limit of our current measurement for voltages smaller than ~1 V. The small

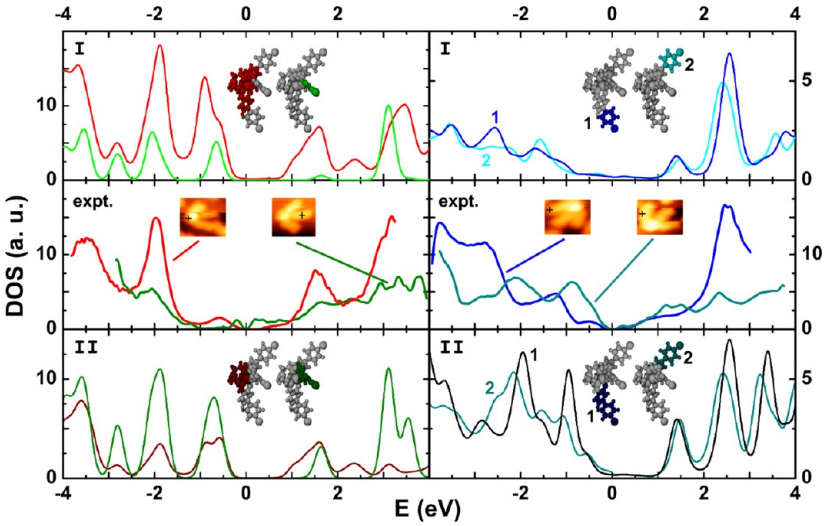

Figure 7. Comparison of calculated and measured local DOS. Distribution I is shown in the upper panel; distribution II in the lower panel. The middle panel shows experimental curves. Experimental and theoretical local DOS are in good general agreement. They indicate that spectra on the middle leg (green) result in a measurement of distribution II. In contrast for leg 1/2 (right-hand side) the measured spectra resemble distribution I or II depending on the tip position.

"peak" at −0.3 eV, therefore, is an artifact of noise at the resolution limit, while the peak at −2 eV is real and regularly found. We always find multiple peaks or a broad structure above +3 eV. This is plausible because due to the protruding legs geometry it is hardly possible to measure configuration I.

For the two side legs the situation is different. In the occupied states we see a clear difference in the spectra if we tunnel in a position at the very end of the elongated feature (leg) or further toward the bright head dot. In the first case the measured spectrum (blue) resembles much more the theoretical spectra of distribution I (upper panel), while the curve in dark cyan resembles rather the theoretical spectra of distribution II. Obviously, we mainly address the lower phenyl ring when the tip is positioned at the very end of the elongated feature, but we measure contributions from both phenyl rings when we position the tip more toward the bright dot. Even if one is tempted to state that the shown curves rather resemble the calculations of leg 1, the energy resolution of our measurements does not really allow for such conclusions. For example, the broad peak in the dark cyan curve could be the single peak at −2 eV of leg 1; it could, as well, be interpreted as the envelope of the peaks −1.5 eV, −2 eV, and −2.6 eV of leg 2. Similarly, for unoccupied states we observe an effect of the tip position on the spectra, but it is not possible to distinguish leg 1 and leg 2 unambigously with the energy resolution of the tip at room temperature.

CONCLUSIONS

We were able to synthesize a three-dimensional molecule with three identical molecular wires in a nonplanar configuration that assume different orientations upon deposition on a gold surface entailing different couplings and accordingly electronic structures of the wires. This orientation-dependent electronic behavior has been studied by STS. Locally resolved DOS spectra on tilted molecules show large differences between the two wires very close to the surface and the third wire protruding from the surface. The experiments suggest the existence of orbitals located on the head complex and the protruding leg, while at the same energies no orbitals are found for the legs coupled to the surface. Our DFT calculations show that the surface acts on the whole molecule by an overall shift of the DOS spectrum, which can be interpreted as an adjustment of the chemical potential of molecule and surface. However, orbitals that are close to the surface, *e.g.*, those on the phenyl rings of the side legs, undergo an additional energy shift due to the interaction with the surface, while those on the protruding leg do not show an additional shift. Furthermore, some orbitals that originally are located on the lower phenyl ring of the molecule are considerably surpressed by the interaction with the surface. These strong effects are rather due to the interaction with the electronic system of the surface than due to rearrangements within the molecule upon distortion from the isolated conformation. The calculations enable us to establish a correlation of the features observed in the STM images with the actual location of the chemical groups of the molecule. In conclusion, by a concerted effort of chemical synthesis, STM investigations, and quantum chemical calculations we are able to characterize the effect of orientational varying coupling on the electronic properties of a certain molecular wire. This implies that for future multiterminal molecules or molecules containing several functional units special care has to be taken in designing the connecting wires. Their conformation

within the molecular module and their final conformation in the deposited module are of similar importance as is the design of the functional units. Furthermore, our results show that the switching of the electronic properties of a molecular wire may be acchieved not only due to a change of chemical bonds within the wire molecule but as well or solely due to a reorientation of the whole wire.

METHODS

Preparation of Samples. The surface of an Au(111) single crystal was cleaned in ultra-high vacuum (UHV) by repeated Ar^+ ion bombardment and subsequent annealing to $T = 820$ K. A droplet of molecule solution ($c \approx 2 \times 10^{-6}$ mol/L in CH_2Cl_2) was put on the surface in the opened load lock of the chamber while a steady flow of N_2 was maintained to prevent contamination from air. The load lock was then closed and evacuated immediately. CH_2Cl_2 evaporates within a few seconds. Remaining solvent molecules can be removed from the surface by annealing the sample at $T = 323$ K for 10 min in UHV. The sample was then transferred to the precooled STM.

STM and STS Measurements. A modified Omicron VT UHV STM equipped with a Femto preamplifier was used. Switching from SCALA to Nanonis electronics did not change the basic outcome of imaging and STS. Tips were electrochemically etched from tungsten wire and cleaned *in situ* before each experiment by repeated annealing and sputtering cycles. All STM images were recorded in the constant-current mode with the sample at $T \approx 30$ K. For spectroscopy the tip was placed at well-defined locations above the molecule, the position was fixed (always maintaining a vacuum gap between tip and sample), and the voltage ramped from $V = 0$ to negative or positive voltages while the current I was monitored. $I(V)$ curves were discarded if imaging indicated an alteration of molecule or tip afterward. $I(V)$ curves that show an obvious reconfiguration of the tip (current jump) while the molecule was found to be unharmed were regarded only well below the jump. This procedure requires collection and control of STM images before and after a spectrum is taken. It slows down the measurements as well as the data processing as compared to a "blind" repetition and averaging over all measured curves. We regard our procedure essential in order to gain insight into the basic molecular conduction processes.

Deconvolution of the Density of States. For the rather large voltage ranges used in the spectroscy of molecules, dI/dV cannot be interpreted as a quantity proportional to the sample's local DOS.[13,40−42] Instead the DOS has to be deconvolved.[35−38] We follow the approach of Wagner *et al.*, which takes into account the full trapezoidal shape of the tunneling barrier in the one-dimensional Wentzel−Kramers−Brillouin approximation for the transmission coefficient (eq 3 in ref 35). The DOS is obtained by a recursion formula (eq 13 in ref 35). We chose ΔV as used for the measurements, and $I(V)$ curves were smoothed before the calculation of dI/dV and DOS. We assumed $\Phi_S = \Phi_T = 5$ eV for the work function. The expression for the tip−surface distance was varied between 0.35 and 0.55 nm, which allows for averaging spectra measured at different tunneling set point values I and V.

Statistics. To estimate a probability for different molecule orientations on the gold surface, we used a simplistic model: In order to position two sulfur atoms of the molecule in identical positions on gold, the S−S distance of the isolated molecule of 17.28 Å has to be expanded or compressed by δ. This will cause a change in energy of $\Delta E = (1/2)D\delta^2$, which results in a probabilty for this expanded/compressed configuration of $a_0 \exp(-\Delta E/kt)$. In Figure 3(c) the resulting probabilities are indicated for two configurations. The prefactor a_0 has been adjusted to fit the heights of measurements. The stretching energy has been chosen as $(1/2)D = 1$ meV/Å^2, which is on the order of the stretching energies of molecules.

DFT Calculations. Quantum chemical calculations were performed on the molecule in different conformations and surroundings. As a surface an extended gold cluster (two layers, 100 atoms each) was used that resembles an unreconstructed gold(111) surface. All calculations were performed with the program package TURBOMOLE.[43] The gradient-corrected BP86 functional[44,45] was used throughout. The atoms of the molecule were equipped with a def2-SVP basis set.[46] For the core (inner 60 electrons) of the Au atoms a Dirac−Hartree−Fock electronic core potential[47] in combination with the def-SVP basis set was used. The resolution of the identity approximation was used throughout. For the interaction of the phenyl rings of the adsorbed molecule with the gold surface van der Waals interactions are crucial, as has been shown, for example, in refs 48 and 49. They have been taken into account by the DFT-D3 approximation with Becke−Johnson damping in all calculations.[50,51] In the structure optimizations all atoms of the molecule were allowed to relax, while the gold positions were fixed. The starting configuration for the free molecule was taken from the crystal structure obtained by X-ray defraction. Only minor changes were observed for the optimized structure of the free molecule, while the adsorbed molecule is heavily distorted by the surface. Our calculations focused on the electronic structure of the adsorbed molecule close to the Fermi level. About 900 orbitals are located in the range of 5 eV below the Fermi level (HOMO energy of the full system: gold cluster + molecule), which is located at −5.17 eV. In the range of 5 eV above the Fermi level about 200 orbitals are found. The simulation of the local density of states on the molcule was based on an orbital-resolved Mulliken population analysis[52] The DOS of the whole molecule was than simulated by the following procedure: For each orbital the Mulliken populations of the molecular atoms were added. Because of the finite system size we obtain a line spectrum of populations at discrete orbital energies. In the next step, this discrete spectrum was broadened by a Gauss convolution with a constant peak width of 0.3 eV. For the calculation of a local DOS the summation comprised only atoms of a certain section of the molecule (*e.g.*, legs, head). The Fermi energy in the caclulations of the free molecule lies at −4.635 eV. To compare to the STM data all calculated spectra have been shifted by 4.635 eV, to adjust E_F to $U = 0$ V.

It is well known that DFT tends to underestimate HOMO−LUMO gaps in semiconductors.[53] However, for molecules the error in the HOMO−LUMO gap seems to be much smaller and the sign cannot be predicted.[54] In our investigation we combine a metal cluster, where we correctly obtain no band gap at all, and a molecule. Furthermore, the lowest unoccupied orbitals of the molecule are π^* orbitals of the phenyl rings (valence orbitals), which are comparably well described in the calculations. Finally, we compared the HOMO−LUMO gap of the molecule (2.02 eV) with the enery difference between the ground state and the lowest triplet state (2.04 eV), which can be obtained by a DFT ground-state calculation for spin = 1 and therefore is completely independent from the definition of orbital energies. From the latter calculation we also obtain orbital energies. In this case the LUMO orbital of the ground state is occupied as well, and the problem of a different treatment of HOMO and LUMO is avoided. The energy difference of the two highest occupied alpha (majority spin) orbitals (which correspond to HOMO and LUMO of the ground state) amounts to an energy difference of 2.21 eV, which is again in the same range. We conclude that for the given system the error of the HOMO−LUMO gap is comparably small.

Conflict of Interest: The authors declare no competing financial interest.

Acknowledgment. M.L. and M.M. acknowledge financial support by the Baden-Württemberg Stiftung. We thank W. Wulfhekel, V. Meded, and F. Evers for many fruitful discussions.

REFERENCES AND NOTES

1. Reed, M. A.; Zhou, C.; Muller, C. J.; Burgin, T. P.; Tour, J. M. Conductance of a Molecular Junction. *Science* **1997**, *278*, 252–254.
2. Cui, X. D.; Primak, A.; Zarate, X.; Tomfohr, J.; Sankey, O. F.; Moore, A. L.; Moore, T. A.; Gust, D.; Harris, G.; Lindsay, S. M. Reproducible Measurement of Single-Molecule Conductivity. *Science* **2001**, *294*, 571–574.
3. Bumm, L. A.; Arnold, J. J.; Cygan, M. T.; Dunbar, T. D.; Burgin, T. P.; Jones, L., II; Allara, D. L.; Tour, J. M.; Weiss, P. S. Are Single Molecular Wires Conducting? *Science* **1996**, *271*, 1705–1707.
4. Reichert, J.; Ochs, R.; Beckmann, D.; Weber, H.; Mayor, M.; v. Löhneysen, H. Driving Current through Single Organic Molecules. *Phys. Rev. Lett.* **2002**, *88*, 176804.
5. Xu, B.; Tao, N. J. Measurement of Single-Molecule Resistance by Repeated Formation of Molecular Junctions. *Science* **2003**, *301*, 1221–1223.
6. Venkataraman, L.; Klare, J. E.; Nuckolls, C.; Hybertsen, M. S.; Steigerwald, M. L. Dependence of Single-Molecule Junction Conductance on Molecular Conformation. *Nature* **2006**, *442*, 904–907.
7. Lörtscher, E.; Weber, H.; Riel, H. Statistical Approach to Investigating Transport through Single Molecules. *Phys. Rev. Lett.* **2007**, *98*, 176807.
8. Akkerman, H.; de Boer, B. Electrical Conduction through Single Molecules and Self-Assembled Monolayers. *J. Phys.: Condens. Matter* **2008**, *20*, 0130001.
9. Kiguchi, M.; Kaneko, S. Single Molecule Bridging between Metal Electrodes. *Phys. Chem. Chem. Phys.* **2013**, *15*, 2253–2267.
10. Landau, A.; Kronik, L.; Nitzan, A. Cooperational Effects in Molecular Conduction. *J. Comput. Theor. Nanosci.* **2008**, *5*, 535–544.
11. Li, C.; Pobelov, I.; Wandlowski, T.; Bagrets, A.; Arnold, A.; Evers, F. Charge Transport in Single Au/Alkanedithiol/Au Junctions: Coordination Geometries and Conformational Degrees of Freedom. *J. Am. Chem. Soc.* **2008**, *130*, 318–326.
12. Lafferentz, L.; Ample, F.; Yu, H.; Hecht, S.; Joachim, C.; Grill, L. Conductance of a Single Conjugated Polymer as a Continuous Function of its Length. *Science* **2009**, *323*, 1193.
13. Néel, N.; Kröger, J.; Limot, L.; Berndt, R. Conductance of Oriented C_{60} Molecules. *Nano Lett.* **2008**, *8*, 1291–1295.
14. Wang, Y. F.; Kröger, J.; Berndt, R.; Vázquez, H.; Brandbyge, M.; Paulson, M. Atomic-Scale Control of Electron Transport through Single Molecules. *Phys. Rev. Lett.* **2010**, *104*, 176802.
15. Schmaus, S.; Bagrets, A.; Nahas, Y.; Yamada, T. K.; Bork, A.; Bowen, M.; Beaurepaire, E.; Evers, F.; Wulfhekel, W. Giant Magnetoresistance through a Single Molecule. *Nat. Nanotechnol.* **2011**, *6*, 185–189.
16. Makk, P.; Tomaszewski, D.; Martinek, J.; Balogh, Z.; Csonka, S.; Wawrzyniak, M.; Frei, M.; Venkataraman, L.; Halbritter, A. Correlation Analysis of Atomic and Single-Molecule Junction Conductance. *ACS Nano* **2012**, *6*, 3411–3423.
17. Mishchenko, A.; Vonlanthen, D.; Meded, V.; Bürkle, M.; Li, C.; Pobelov, I. V.; Bagrets, A.; Viljas, J. K.; Pauly, F.; Evers, F.; *et al.* Influence of Conformation on Conductance of Biphenyl-Dithiol Single-Molecule Contacts. *Nano Lett.* **2010**, *10*, 156–163.
18. Ie, Y.; Hirose, T.; Nakamura, H.; Kiguchi, M.; Takagi, N.; Kawai, M.; Aso, Y. Nature of Electron Transport by Pyridine-Based Tripodal Anchors: Potential for Robust and Conductive Single-Molecule Junctions with Gold Electrodes. *J. Am. Chem. Soc.* **2011**, *133*, 3014–3022.
19. Peng, Z.-L.; Chen, Z.-B.; Zhou, X.-Y.; Sun, Y.-Y.; Liang, J.-H.; Niu, Z.-J.; Zhou, X.-S.; Mao, B.-W. Single Molecule Conductance of Carboxylic Acids Contacting Ag and Cu Electrodes. *J. Phys. Chem. C* **2012**, *116*, 21699–21705.
20. Stipe, B. C.; Rezaei, M. A.; Ho, W. Localization of Inelastic Tunneling and the Determination of Atomic-Scale Structure with Chemical Specificity. *Phys. Rev. Lett.* **1999**, *82*, 1724–1727.
21. Lukas, M.; Kelly, R. E. A.; Kantorovich, L. N.; Otero, R.; Xu, W.; Lægsgaard, E.; Stensgaard, I.; Besenbacher, F. Adenine Monolayers on the Au(111) Surface: Structure Identification by Scanning Tunneling Microscopy Experiment and *ab Initio* Calculations. *J. Chem. Phys.* **2009**, *130*, 024705.
22. Néel, N.; Kröger, J.; Berndt, R. Two-Level Conductance Fluctuations of a Single-Molecule Junction. *Nano Lett.* **2011**, *11*, 3593–3596.
23. Moresco, F.; Gross, L.; Alemani, M.; Rieder, K.-H.; Tang, H.; Gourdon, A.; Joachim, C. Probing the Different Stages in Contacting a Single Molecular Wire. *Phys. Rev. Lett.* **2003**, *91*, 036601.
24. Hirayama, D.; Takimiya, K.; Aso, Y.; Otsubo, T.; Hasobe, T.; Yamada, H.; Imahori, H.; Fukuzumi, S.; Sakata, Y. Large Photocurrent Generation of Gold Electrodes Modified with [60]Fullerene-Linked Oligothiophenes Bearing a Tripodal Rigid Anchor. *J. Am. Chem. Soc.* **2002**, *124*, 532–533.
25. Jian, H.; Tour, J. M. En Route to Surface-Bound Electric Field-Driven Molecular Motors. *J. Org. Chem.* **2003**, *68*, 5091–5103.
26. Wei, L.; Padmaja, K.; Youngblood, W. J.; Lysenko, A. B.; Lindsey, J. S.; Bocian, D. F. Diverse Redox-Active Molecules Bearing Identical Thiol-Terminated Tripodal Tethers for Studies of Molecular Information Storage. *J. Org. Chem.* **2004**, *69*, 1461–1469.
27. Takamatsu, D.; Yamakoshi, Y.; Fukui, K. Photoswitching Behavior of a Novel Single Molecular Tip for Noncontact Atomic Force Microscopy Designed for Chemical Identification. *J. Phys. Chem. B* **2006**, *110*, 1968–1970.
28. Terada, K.; Kobayashi, K.; Haga, M. Synthesis, Electrochemical, and Molecular Inclusion Properties of 'Canopied' Trinuclear Ruthenium Complexes with Six Anchoring Groups on an ITO Electrode. *Dalton Trans.* **2008**, 4846–4854.
29. Mann, J. A.; Rodríguez-López, J.; Abruña, H. D.; Dichtel, W. R. Multivalent Binding Motifs for the Noncovalent Functionalization of Graphene. *J. Am. Chem. Soc.* **2011**, *133*, 17614–17617.
30. Ramachandra, S.; Schuermann, K. C.; Edafe, F.; Belser, P.; Nijhuis, C. A.; Reus, W. F.; Whitesides, G. M.; De Cola, L. Luminescent Ruthenium Tripod Complexes: Properties in Solution and on Conductive Surfaces. *Inorg. Chem.* **2011**, *50*, 1581–1591.
31. Schramm, A.; Stroh, C.; Dössel, K.; Lukas, M.; Fischer, M.; Schramm, F.; Fuhr, O.; v. Löhneysen, H.; Mayor, M. Tripodal M(III) Complexes on Au(111) Surfaces: Towards Molecular 'Lunar Modules'. *Eur. J. Inorg. Chem.* **2013**, *2013*, 70–79.
32. Schramm, A.; Stroh, C.; Dössel, K.; Lukas, M.; Fuhr, O.; v. Löhneysen, H.; Mayor, M. Isolated Facial and Meridonial Tris(bipyridine)Ru(II) for STM Studies on Au(111). *Chem. Commun.* **2013**, *49*, 1076–1078.
33. Wöll, C.; Chiang, S.; Wilson, R. J.; Lippel, P. H. Determination of Atom Positions at Stacking-Fault Dislocations on Au(111) by Scanning Tunneling Microscopy. *Phys. Rev. B* **1989**, *39*, 7988–7991.
34. Pan, G.-B.; Mann, O.; Freyland, W. Nanoscale Electrodeposition of Ga on Au(111) from Ionic Liquids. *J. Phys. Chem. C* **2011**, *115*, 7656–7659.
35. Wagner, C.; Franke, R.; Fritz, T. Evaluation of *I*(*V*) Curves in Scanning Tunneling Spectroscopy of Organic Layers. *Phys. Rev. B* **2007**, *75*, 235432.
36. Passoni, M.; Donati, F.; Li Bassi, A.; Casari, C. S.; Bottani, C. E. Recovery of Local Density of States Using Scanning Tunneling Spectroscopy. *Phys. Rev. B* **2009**, *79*, 045404.
37. Ziegler, M.; Néel, N.; Sperl, A.; Kröger, J.; Berndt, R. Local Density of States from Constant-Current Tunneling Spectra. *Phys. Rev. B* **2009**, *80*, 125402.
38. Koslowski, C.; Pfeifer, H.; Ziemann, P. Deconvolution of the Electronic Density of States of Tip and Sample from Scanning Tunneling Spectroscopy Data: Proof of Principle. *Phys. Rev. B* **2009**, *80*, 165419.
39. Repain, V.; Berroir, J. M.; Rousset, S.; Lecoeur, J. Interaction between Steps and Reconstruction on Au(111). *Europhys. Lett.* **1999**, *47*, 435–441.
40. Stroscio, J. A.; Feenstra, R. M.; Fein, A. P. Electronic Structure of the Si(111) 2 × 2 Surface by Scanning-Tunneling Microscopy. *Phys. Rev. Lett.* **1986**, *57*, 2579–2582.
41. Schöck, M.; Sürgers, C.; v. Löhneysen, H. Atomically Resolved Tunneling Spectroscopy on Si(557)-Au. *Europhys. Lett.* **2006**, *74*, 473–478.

42. Takács, A. F.; Witt, F.; Schmaus, S.; Balashow, T.; Bowen, M.; Beaurepaire, E.; Wulfhekel, W. Electron Transport through Single Phtalocyanine Molecules Studied Using Scanning Tunneling Microscopy. *Phys. Rev. B* **2008**, *78*, 233404.
43. *TURBOMOLE V6.4 2012*; a development of University of Karlsruhe and Forschungszentrum Karlsruhe GmbH, 1989–2007; TURBOMOLE GmbH, since 2007; available from http://www.turbomole.com.
44. Becke, A. D. Density-Functional Exchange-Energy Approximation with Correct Asymptotic Behavior. *Phys. Rev. A* **1988**, *38*, 3098–3100.
45. Perdew, J. P. Density-Functional Approximation for the Correlation Energy of the Inhomogeneous Electron Gas. *Phys. Rev. B* **1986**, *33*, 8822–8824.
46. Weigend, F.; Ahlrichs, R. Balanced Basis Sets of Split Valence, Triple Zeta Valence and Quadruple Zeta Valence Quality for H to Rn: Design and Assessment of Accuracy. *Phys. Chem. Chem. Phys.* **2005**, *7*, 3297–3305.
47. Figgen, D.; Rauhut, G.; Dolg, M.; Stoll, H. Energy-Consistent Pseudopotentials for Group 11 and 12 Atoms: Adjustment to Multi-Configuration Dirac-Hartree-Fock Data. *Chem. Phys.* **2005**, *311*, 227–244.
48. Tonigold, K.; Groß, A. Adsorption of Small Aromatic Molecules on the (111) Surfaces of Noble Metals: A Density Functional Theory Study with Semiempirical Corrections for Dispersion Effects. *J. Chem. Phys.* **2010**, *132*, 224701.
49. Lange, H.; Maultzsch, J.; Meng, W.; Mollenhauer, D.; Paulus, B.; Peica, N.; Schlecht, S.; Thomsen, C. Adsorption Behavior of 4-Methoxypyridine on Gold Nanoparticles. *Langmuir* **2011**, *27*, 7258–7264.
50. Grimme, S.; Antony, J.; Ehrlich, S.; Krieg, H. A Consistent and Accurate *ab Initio* Parametrization of Density Functional Dispersion Correction (DFT-D) for the 94 Elements H-Pu. *J. Chem. Phys.* **2010**, *132*, 154104.
51. Grimme, S.; Ehrlich, S.; Goerigk, L. Effect of the Damping Function in Dispersion Corrected Density Functional Theory. *J. Comput. Chem.* **2011**, *32*, 1456–1465.
52. Mulliken, R. S. Electronic Population Analysis on LCAO-MO Molecular Wave Functions. I. *J. Chem. Phys.* **1955**, *23*, 1833–1840.
53. Perdew, J. P.; Levy, M. Physical Content of the Exact Kohn-Sham Orbital Energies: Band Gaps and Derivative Discontinuities. *Phys. Rev. Lett.* **1983**, *51*, 1884–1887.
54. Zhang, G.; Musgrave, C. B. Comparison of DFT Methods for Molecular Orbital Eigenvalue Calculations. *J. Phys. Chem. A* **2007**, *111*, 1554–1561.